Nonlinear Dyn
https://doi.org/10.1007/s11071-025-11250-9

RESEARCH

Nonlinear model predictive control of trajectory tracking for autonomous trucks with terminal ingredients

Wenbo Li · Shuyou Yu · Baojun Lin · Hong Chen

Received: 16 December 2024 / Accepted: 13 April 2025

Abstract Model predictive control (MPC) without guaranteed stability is typically employed for trajectory tracking of autonomous trucks (ATs). However, in certain scenarios, the tracking error may fail to converge. To address this, the optimization control problem can be designed by incorporating terminal ingredients, i.e., the terminal control gain, terminal constraint, and terminal cost function. In this paper, we propose a nonlinear model predictive control (NMPC) scheme with terminal ingredients for trajectory tracking of ATs in the presence of the coupled longitudinal and lateral dynamics. The trajectory tracking problem exhibits asymptotic convergence, and the optimization control problem (OCP) ensures recursive feasibility. The complexity of the proposed controller is similar to that of a standard NMPC without terminal ingredients. Additionally, we introduce an efficient Newton-type method with a look-up table (NTLT) to solve the OCP. Co-simulations in Matlab/Simulink and TruckSim validate the effectiveness of the proposed NMPC scheme and the NTLT across various scenarios.

Keywords Autonomous truck · Trajectory tracking · Nonlinear model predictive control · Recursive feasibility · Asymptotic convergence · Newton-type method

W. Li · S. Yu
National Key Laboratory of Automotive Chassis Integration and Bionics, Jilin University, Changchun, China
e-mail: liwb21@mails.jlu.edu.cn

W. Li · S. Yu (✉) · B. Lin
Department of Control Science and Engineering, Jilin University, Changchun, China
e-mail: Shuyou@jlu.edu.cn

B. Lin
e-mail: linbj@jlu.edu.cn

H. Chen
College of Electronics and Information Engineering, Tongji University, Shanghai, China
e-mail: chenhong2019@tongji.edu.cn

1 Introduction

Autonomous vehicles (AVs) have seen significant advancements in the transportation industry, offering significant benefits such as enhanced road safety, improved transportation efficiency, and reduced fuel consumption [1]. As an important part of the intelligent transportation system, autonomous trucks (ATs) still face considerable challenges due to their large mass and complex nonlinear dynamics.

Trajectory tracking control is a key technology in autonomous driving systems [2]. In [3], a sliding mode controller is proposed for parking control, adopting a kinematic model. In [4–6], proportional-integral-derivative (PID) controllers are designed for the longitudinal control of vehicle platooning. However, kinematic model-based controllers are typically applied for AVs at low velocities or with low mass. Considering the nonlinear vehicle dynamics, some controllers have been extensively developed for trajectory tracking of

Published online: 09 May 2025

AVs. In [7–10], sliding mode controllers are proposed to guarantee that tracking errors asymptotically converge to zero. In [11,12], backstepping controllers are designed for the steering control of AVs, considering the lateral vehicle dynamics. In [13], a coupled longitudinal and lateral dynamic inverse model is established for trajectory tracking. However, the above studies do not handle the constraints on states and inputs of vehicle systems, which may lead to driving instability.

Model predictive control (MPC) has been widely developed for trajectory tracking in AVs, offering significant advantages in effectively managing constraints and nonlinear vehicle dynamics. A comprehensive review of MPC-based controllers for AVs is provided in [14]. In [15], an adaptive reduced-horizon MPC is proposed to reduce computational time during trajectory tracking. To ensure the stability of the closed-loop system, i.e., to guarantee that the tracking errors asymptotically converge to zero, a tube-based MPC is introduced in [16], employing a kinematic bicycle model as the prediction model. In [17], a MPC with PID feedback is proposed to improve the tracking accuracy and steering smoothness compared to that of the conventional MPC. Several representative studies based on vehicle dynamics models are summarized in Table 1. In [18–23], nonlinear model predictive control (NMPC) is designed considering the nonlinear vehicle dynamics, which is essential for enhancing the accuracy of predictive values. However, in certain scenarios, the trajectory tracking control objective may not be achieved due to the inability to guarantee the stability of the vehicle control system. To account for system uncertainties, a tube-based MPC is developed in [24–26], where a linear parameter-varying (LPV) vehicle dynamics model is utilized as the prediction model. In [27], a linear MPC approach based on Koopman operator theory is proposed for truck platooning, ensuring the stability and recursive feasibility by incorporating terminal constraints. However, linearized models still face inherent uncertainties. Consequently, Lyapunov-based NMPC has been proposed to ensure the stability of autonomous underwater vehicle control systems [28–30]. However, this approach primarily considers input constraints. In [31], an NMPC with a sufficiently long horizon is proposed for trajectory tracking in ATs. However, determining the appropriate prediction horizon to guarantee closed-loop stability remains a challenge. In addition, a longer prediction horizon leads to increased computation time [32].

Furthermore, real-time implementation of NMPC should be considered in ATs. Significant studies have been proposed to reduce the computational burden of NMPC. Some studies focus on simplifying models (e.g., Jacobian linearization model or Koopman operator model [27]), while others exploit banded structures of the optimization problem, such as the multiple shooting method [33], parallel computing approaches [34], and so on. In particular, to reduce the computational burden by simplifying models, look-up table-based modeling methods have been proposed. Generally, look-up tables are generated by the block diagram of systems. In [35], a MPC scheme is designed for Hammerstein systems, where look-up tables are generated to represent the static block. A two-layer control strategy is proposed in [36], where a look-up table is used in the upper layer to determine steady states, while an unconstrained MPC is employed to track the steady states in the lower layer. In [37], an NMPC scheme is proposed for four-wheel steering vehicles, where look-up tables of tires are designed to reduce the computational burden under heuristic algorithms. Moreover, Newton-type (NT) methods have garnered significant attention, which can be further categorized into sequential quadratic programming and interior-point methods depending on how to handle constraints. Under the framework of NT method, by simplifying the Jacobian matrix, either Riccati NT recursion or parallel NT methods have been proposed [38].

Motivated by the analysis above, this paper proposes an NMPC scheme for reference trajectory tracking of ATs. Furthermore, an improved Newton-type method with a look-up table (NTLT) for solving the optimization problem is presented. The key contributions of this paper are as follows:

1. Considering the coupled longitudinal and lateral dynamics of trucks, an NMPC with terminal ingredients is formulated to guarantee recursive feasibility and asymptotic convergence. Simulation results show that an NMPC without terminal ingredients cannot guarantee asymptotic convergence to the reference trajectory. Furthermore, the complexity of the proposed NMPC is similar to that of nominal NMPC without terminal ingredients.
2. To ensure the real-time implementation of the proposed NMPC, the NTLT algorithm with a look-up table for tires is proposed to reduce the computa-

Table 1 Literature on trajectory tracking for autonomous vehicles based on MPC

	Linear dynamic	Nonlinear dynamic	Statibility	State constraint	Input constraint
[18]		✓			✓
[19–23]		✓		✓	✓
[24–26]	✓		✓	✓	✓
[27]	✓		✓	✓	✓
[28–30]		✓	✓		✓
[31]		✓	✓	✓	✓

tional burden caused by the nonlinear truck dynamics.

The remainder of this paper is structured as follows: Sect. 2 presents the truck dynamics. Section 3 describes the control strategy. Section 4 introduces the NTLT. Section 5 evaluates the control strategy. Finally, conclusions are drawn in Sect. 6.

1.1 Basic notations

Let $\mathbb{R}$ denote the set of real numbers. The symbol $\|x\|$ represents the Euclidean norm, and $\|x\|_Q = \sqrt{x^T Qx}$ for any vector $x \in \mathbb{R}^n$, where $Q \in \mathbb{R}^{n\times n}$ is positive definite. For a matrix M, the notation $M \succeq 0$ indicates that M is positive semi-definite. For a variable $a \in \mathbb{R}^1$, a_{min} and a_{max} represent its minimum and maximum values, respectively. The term $i\,|k$ indicates the predicted value at the future time instant $k+i$ starting from the current time instant k. The symbol $*$ signifies the transpose of a matrix block located symmetrically within the matrix, $\mathbf{0}$ represents a zero matrix of appropriate dimensions, I represents a unit matrix of appropriate dimensions, $\lfloor\cdot\rfloor$ represents the floor function, i.e., the argument is rounded down to the closest integer, and $diag\,(e_1,\ldots,e_n)$ is a diagonal matrix with diagonal elements e_1 to e_n. Given sets $E \in \mathbb{R}^n$ and $S \in \mathbb{R}^n$, $\mathrm{E} \oplus S = \{e+s\,|e \in E, s \in S\}$ is the Minkowski sum, $\mathrm{E} \ominus S = \{e\,|e+s \in E, \forall s \in S\}$ is the Pontryagin difference, and $\mathrm{E} \circ S = \{e \times s\,|e \in E, s \in S\}$.

2 Truck dynamics

As shown in Fig. 1, a light-duty bicycle-truck with four tires on the rear driving axle is presented, where v_x is the longitudinal velocity, v_y is the lateral velocity, γ is the yaw rate, F_{xr} is the longitudinal force of the rear tire, F_{yf} is the lateral force of the front tire, F_{yr} is the lateral force of the rear tire, m is the truck mass, I_z is the yaw moment of inertia, l_f and l_r are the distances from the center of gravity to the front and rear axles, respectively.

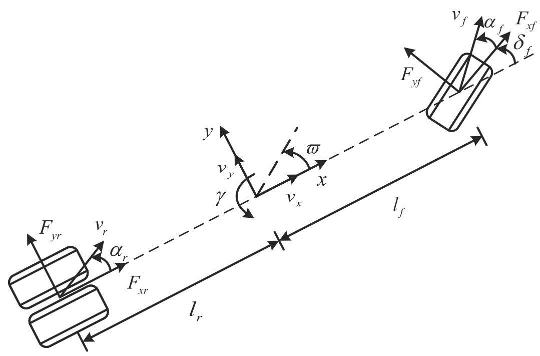

Fig. 1 Truck with 4x2 axle configuration

Then, a 3-DOF bicycle model of ATs including the longitudinal, lateral, and yaw motions is presented as [39]

$$\begin{cases} \dot{v}_x = v_y\gamma + \frac{F_{xr}}{m}, \\ \dot{v}_y = -v_x\gamma + \frac{1}{m}\left(F_{yf} + F_{yr}\right), \\ \dot{\gamma} = \frac{1}{I_z}\left(l_f F_{yf} - l_r F_{yr}\right). \end{cases} \tag{1}$$

The Magic Formula tire model of the rear axle is [40]

$$\begin{aligned} F_{yf} &= f_t\left(\alpha_f\right) \\ &= D_f \sin\left[C_f \arctan\left\{B_f\alpha_f - E_f\left(B_f\alpha_f\right.\right.\right. \\ &\qquad \left.\left.\left. - \arctan\left(B_f\alpha_f\right)\right)\right\}\right], \end{aligned} \tag{2}$$

where α_f is the slip angle of the front tire, and B_f, C_f, D_f, and E_f are constants.

In Fig. 2, $F_{yfmin} = f_t\left(\alpha_{fmin}\right)$ and $F_{yfmax} = f_t\left(\alpha_{fmax}\right)$ represent the maximum and minimum values of the lateral force of the front tire, respectively.

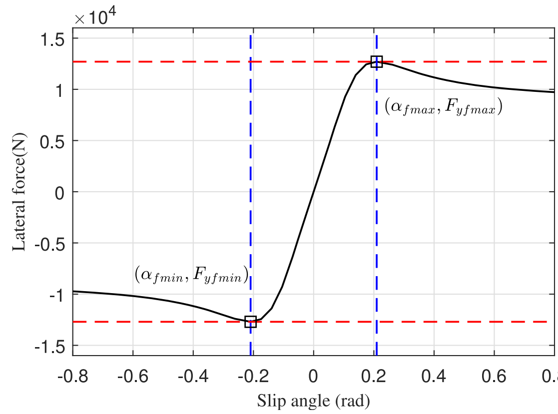

Fig. 2 Magic Formula tire model

Denote the state vector $x = [v_x, v_y, \gamma]^T$ and the input vector $u = [F_{xr}, \alpha_f, F_{yr}]^T$. Note that the control inputs can be converted to steering wheel angles and rear wheel torques [13]. For the sake of simplicity, the process of conversion is omitted.

Then, by the Euler method, the truck model in (1) can be discretized with a sampling time t_s as

$$x(k+1) = f(x(k), u(k)), \tag{3}$$

where $k = \lfloor t/t_s \rfloor$ is the time instant.

Furthermore, the state x and control input u should satisfy the following constraints

$$x \in \mathcal{X} := \left\{ x \in \mathbb{R}^3 \left| \begin{array}{l} v_{xmin} \le v_x \le v_{xmax}, \\ v_{ymin} \le v_y \le v_{ymax}, \\ \gamma_{\min} \le \gamma \le \gamma_{\max}. \end{array} \right. \right\}, \tag{4}$$

and

$$u \in \mathcal{U} := \left\{ u \in \mathbb{R}^3 \left| \begin{array}{l} F_{xrmin} \le F_{xr} \le F_{xrmax}, \\ \alpha_{fmin} \le \alpha_f \le \alpha_{fmax}, \\ F_{yrmin} \le F_{yr} \le F_{yrmax}. \end{array} \right. \right\}. \tag{5}$$

By (2) and (5), the constraint of the lateral force of the front tire is defined as

$$F_{yf} \in \mathscr{F}_{yf} := \left\{ F_{yf} \in \mathbb{R}^1 | F_{yfmin} \le F_{yf} \le F_{yfmax} \right\}. \tag{6}$$

Note that $f_t(\alpha_f)$ is bijective for $x \in \mathcal{X}$, i.e., there always exists $\alpha_f \in \mathcal{U}$ if $F_{yf} \in \mathscr{F}_{yf}$.

Remark 1 The truck considered in this paper and passenger vehicles have similar dynamics. However, in general, trucks have a larger mass and a higher center of gravity compared to passenger vehicles. As a result, trucks may suffer from problems of handling stability in high-speed driving scenarios.

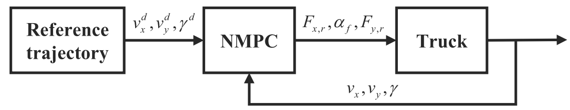

Fig. 3 The control system of ATs

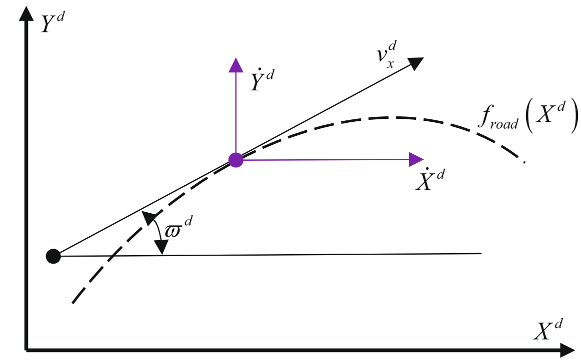

Fig. 4 Reference trajectory

3 Control strategy design

The control objective of ATs is to track a predefined reference trajectory. As shown in Fig. 3, the control system includes two modules: (1) The reference trajectory module generates desired states, i.e., the desired longitudinal velocity v_x^d, lateral velocity v_y^d, and yaw rate γ^d; (2) The NMPC is to track the desired states, where the control inputs are the sideslip angle of the front tire, longitudinal force of the rear tire F_{xr}, and lateral force of the rear tire F_{yr}.

3.1 Reference trajectory

Considering traffic efficiency, handling stability, and passenger comfort, reference trajectory planners have been proposed for ATs in [13]. As shown in Fig. 4, the reference trajectory can be expressed as

$$Y^d = f_{road}\left(X^d\right), \tag{7}$$

where X^d and Y^d are the longitudinal and lateral positions in the global coordinate system, respectively. Note that the function $f_{road} : \mathbb{R}^1 \to \mathbb{R}^1$ is continuously differentiable.

To improve the handling stability of ATs, the desired lateral velocity v_y^d is required to be close to zero, that is, $v_y^d = 0$ [37]. Then, as shown in Fig. 4, according to the kinematic model of trucks, the desired longitudinal velocity v_x^d and the desired yaw rate γ^d of ATs can be derived by [13]

$$\begin{cases} \dot{X}_d = v_x^d \cos\left(\varpi^d\right) \\ \dot{Y}_d = v_x^d \sin\left(\varpi^d\right) \\ \dot{\varphi}^d = \gamma^d \end{cases}, \tag{8}$$

where $\varpi^d = \arctan\left(dY^d/dX^d\right)$.

The desired states can be defined as

$$x^d = p(t), \tag{9}$$

where $p : \mathbb{R}^1 \to \mathbb{R}^3$ is a continuous function with respect to time t and $x^d = \left[v_x^d, v_y^d, \gamma^d\right]^T \in \mathbb{R}^3$.

Furthermore, suppose that the desired states (9) are constrained as

$$x^d \in \mathcal{P} := \left\{x^d \in \mathbb{R}^3 \left| x_{min}^d \le x^d \le x_{max}^d \right.\right\}. \tag{10}$$

The desired states x^d are constrained within the set (4), that is,

$$\mathcal{P} \subseteq \mathcal{X}. \tag{11}$$

Thus, there exists the state $x \in \mathcal{X}$ such that $x = x^d$ for any point x^d on the reference trajectory.

Define the difference between adjacent time instances of the reference trajectory as Δx^d, that is,

$$\Delta x^d(k) = x^d(k) - x^d(k+1). \tag{12}$$

Suppose that Δx^d is constrained

$$\Delta x^d \in \Delta\mathcal{P} := \left\{\Delta x^d \in \mathbb{R}^3 \left| \Delta x_{min}^d \le \Delta x^d \le \Delta x_{max}^d \right.\right\}. \tag{13}$$

3.2 Nonlinear model predictive control

In this section, the tracking problem for the desired states is reformulated into a regulation problem. Subsequently, the OCP with terminal ingredients is formulated.

3.2.1 Desired states tracking problem

Given the desired states x^d in (9), the goal of the trajectory tracking problem is to find an admissible control input u such that [41]

$$\lim_{k\to\infty} \|x_e(k)\| = 0, \tag{14}$$

where

$$x_e(k) = \begin{bmatrix} v_{xe}(k) \\ v_{ye}(k) \\ \gamma_e(k) \end{bmatrix} = \begin{bmatrix} v_x(k) - v_x^d(k) \\ v_y(k) - v_y^d(k) \\ \gamma(k) - \gamma^d(k) \end{bmatrix}. \tag{15}$$

The dynamics of the error system (15) can be described as

$$x_e(k+1) = A(\gamma(k))\, x_e(k) + Bu_e(k), \tag{16}$$

where $B = diag(t_s, t_s, t_s)$, and

$$A(\gamma(k)) = \begin{bmatrix} 1 & t_s\gamma(k) & 0 \\ -t_s\gamma(k) & 1 & 0 \\ 0 & 0 & 1 \end{bmatrix}. \tag{17}$$

Note that, in (16), $A(\gamma(k))$ is a parameter-varying matrix, and u_e is an implicit function of u, x^d, and Δx^d, that is,

$$u_e(k) = \left[u_{e1}(k)\ u_{e2}(k)\ u_{e3}(k)\right]^T, \tag{18}$$

where

$$\begin{cases} u_{e1}(k) = \frac{F_{xr}(k)}{m} + \frac{\Delta v_x^d(k)}{t_s} + \gamma(k)\, v_y^d(k), \\ u_{e2}(k) = \frac{F_{yf}(k)+F_{yr}(k)}{m} + \frac{\Delta v_y^d(k)}{t_s} - \gamma(k)\, v_x^d(k), \\ u_{e3}(k) = \frac{l_f F_{yf}(k) - l_r F_{yr}(k)}{I_z} + \frac{\Delta\gamma^d(k)}{t_s}. \end{cases} \tag{19}$$

By (4) and (10), the constraint set of the error state $x_e \in \mathcal{X}_e$ is defined as

$$\mathcal{X}_e := \left\{x_e \in \mathbb{R}^3 \left| x_{min} - x_{max}^d \le x_e \le x_{max} - x_{min}^d \right.\right\}, \tag{20}$$

where $0 \in \mathcal{X}_e$ by (11).

To establish the constraint set of the control input u_e in (19), by (5), (9), and (13), denote the constraints as $F_{xr} \in \mathscr{F}_{xr}$, $F_{yr} \in \mathscr{F}_{yr}$, $\Delta v_x^d \in \Delta_x$, $\Delta v_y^d \in \Delta_y$, $\Delta\gamma^d \in \Delta_\gamma$, $\gamma \in \Gamma$, $v_x^d \in \Upsilon_x$, and $v_y^d \in \Upsilon_y$, respectively. Therefore, by (19), the constraint of u_e is established as

$$\begin{cases} u_{e1} \in \left\{\frac{\mathscr{F}_{xr}}{m} \oplus \frac{\Delta_x}{t_s} \oplus \Gamma \circ \Upsilon_y\right\}, \\ u_{e2} \in \left\{\frac{\mathscr{F}_{yf} \oplus \mathscr{F}_{yr}}{m} \oplus \frac{\Delta_y}{t_s} \ominus \Gamma \circ \Upsilon_x\right\}, \\ u_{e3} \in \left\{\frac{l_f \mathscr{F}_{yf} \ominus l_r \mathscr{F}_{yr}}{m} \oplus \frac{\Delta_\gamma}{t_s}\right\}. \end{cases} \tag{21}$$

Then, the constraint set of u_e can be expressed as

$$\mathcal{U}_e := \left\{u_e \in \mathbb{R}^3 \left| \begin{array}{l} u_{e1min} \le u_{e1} \le u_{e1max}, \\ u_{e2min} \le u_{e2} \le u_{e2max}, \\ u_{e3min} \le u_{e3} \le u_{e3max} \end{array} \right.\right\}. \tag{22}$$

Note that the constraints of the terms F_{xr}, F_{yf}, F_{yr}, Δv_x^d, and γ in (21) are symmetric. Therefore, the constraint sets (20) and (22) are compact, and $(0, 0) \in \mathcal{X}_e \times \mathcal{U}_e$, indicating that $(0, 0)$ is the equilibrium point of the error system (16). Furthermore, it always holds that there exist control inputs $u \in \mathcal{U}$ and states $x \in \mathcal{X}$ for any $u_e \in \mathcal{U}_e$ and $x_e \in \mathcal{X}_e$ if $x^d \in \mathcal{P}$ and $\Delta x^d \in \Delta\mathcal{P}$. Then, the problem for tracking desired states is reformulated as a regulation problem.

Remark 2 Note that the constraint sets of the state x_e (20) and the control input u_e (22) are used solely for calculating the terminal penalty matrix and terminal constraints.

3.2.2 Optimization control problem

The stage cost function is defined as

$$l\left(x_{e,i|k}, u_{e,i|k}\right) = \left\|x_{e,i|k}\right\|_Q + \left\|u_{e,i|k}\right\|_R,$$

where both $Q \in \mathbb{R}^{3\times 3}$ and $R \in \mathbb{R}^{3\times 3}$ are positive definite weighting matrices.

The OCP of tracking the desired states is formulated as follows:

Problem 1.

$$\underset{U^*(k)}{minimize}\ J\left(x\left(k\right)\right) \tag{23a}$$

subject to

$$x_{0|k} = x\left(k\right), \tag{23b}$$
$$x_{i+1|k} = f\left(x_{i|k}, u_{i|k}\right), \tag{23c}$$
$$x_{e,k+i|k} = x_{k+i|k} - x^d_{k+i|k}, \tag{23d}$$
$$x_{i|k} \in \mathcal{X}, \tag{23e}$$
$$u_{i|k} \in \mathcal{U}, \tag{23f}$$
$$x_{N|k} - x^d_{N|k} \in \mathcal{X}_f, \tag{23g}$$

where

$$J\left(x\left(k\right)\right) = \sum_{i=0}^{N-1} l\left(x_{e,i|k}, u_{e,i|k}\right) + F\left(x_{e,N|k}\right) \tag{24}$$

is the cost function and N is the prediction horizon. The term $\mathcal{X}_f$ is the terminal set, and $F\left(x_{e,N|k}\right)$is the terminal penalty function.

At the time instant k, the optimal solution of Problem 1 is

$$U^*\left(k\right) = \left[u^*_{0|k}, \ldots, u^*_{N-1|k}\right]^T, \tag{25}$$

where the first term $u^*_{0|k}$ represents the current input of ATs. At the subsequent time instant $k+1$, Problem 1 is repeatly solved using the latest state measurements.

Remark 3 Note that the function $l\left(\cdot,\cdot\right) : \mathcal{X}_e \times \mathcal{U}_e \rightarrow \mathbb{R}^1$ is continuous. It satisfies $l\left(0,0\right) = 0$ and $l\left(x_e, u_e\right) > 0$ for all $\left(x_e, u_e\right) \in \mathcal{X}_e \times \mathcal{U}_e \backslash \left\{0, 0\right\}$.

Remark 4 For the trajectory tracking problem of AVs based on the NMPC scheme, the cost function, excluding terminal terms, is typically defined as

$$\tilde{J}\left(x\left(k\right)\right) = \sum_{i=0}^{N-1} \left\|x_{i|k} - x^d_{i|k}\right\|_Q + \left\|u_{i|k}\right\|_R, \tag{26}$$

which may not guarantee asymptotic convergence of the trajectory tracking problem under certain operating conditions [18–23].

We propose a new cost function (24) based on the error system terms (16), and demonstrate that the stability of the trajectory tracking closed-loop system can be ensured with these modifications.

3.2.3 Terminal ingredients

A polytopic linear differential inclusion (PLDI) approach is employed to establish suitable terminal ingredients for Problem 1. For the error system (16), there exists a PLDI Σ such that, for all $x_e \in \mathcal{U}_e$ and $u_e \in \mathcal{U}_e$,

$$A\left(\gamma\left(k\right)\right)x_e + Bu_e \in \Sigma \begin{bmatrix} x_e \\ u_e \end{bmatrix}, \tag{27}$$

where

$$\Sigma := \mathrm{Co}\left\{\left[A\left(\gamma_{\min}\right), B\right], \left[A\left(\gamma_{\max}\right), B\right]\right\}. \tag{28}$$

The constraint set of states and inputs of the error system (16) is redefined within a polytope framework, i.e.,

$$\Xi = \left\{\begin{bmatrix} x_e \\ u_e \end{bmatrix} \in \mathbb{R}^6 \middle| c_j x_e + d_j u_e \leq 1, j = 1, \ldots, p\right\}, \tag{29}$$

where $c_j \in \mathbb{R}^3$ and $d_j \in \mathbb{R}^3$ are two constant vectors.

The terminal ingredients can be derived by solving the following optimization problem [41].

Problem 2.

$$\underset{\Psi\geq 0, Z}{maximize}\left(\det\left(\Psi\right)\right)^{1/3} \tag{30a}$$

subject to

$$\begin{bmatrix} \Psi & * & * & * \\ A\left(\gamma_i\right)\Psi + BZ & \Psi & * & * \\ Q^{1/2}\Psi & 0 & I & * \\ R^{1/2}Z & 0 & 0 & I \end{bmatrix} \succeq \mathbf{0}, \quad i = \{\min, \max\} \tag{30b}$$

$$\begin{bmatrix} \Psi & * \\ c_j\Psi + d_jZ & 1 \end{bmatrix} \succeq \mathbf{0},\ j \in \{1, \dots, p\} \tag{30c}$$

Thus, the terminal control law is $\kappa(x_e) = Z\Psi^{-1}x_e$, the terminal penalty matrix is $P = \Psi^{-1}$, the terminal penalty function is

$$F\left(x_{e,N|k}\right) = \left\|x_{N|k} - x^d_{N|k}\right\|^2_P, \tag{31}$$

and the terminal set is:

$$\mathcal{X}_f = \left\{x_e \in \mathbb{R}^3 \,\middle|\, x_e^T\Psi^{-1}x_e \le 1\right\}. \tag{32}$$

Remark 5 The pair of system matrix of (16) $(A(\gamma), B)$ does not depend on the parameters of the desired states. Consequently, the terminal penalty matrix and terminal set remain constant.

Remark 6 The error system (16) is presented to transform the trajectory tracking problem into a regulation problem. Consequently, the terminal ingredients ensuring both recursive feasibility and asymptotic convergence can be calculated using the error system. Furthermore, the control inputs u can be obtained if the nonlinear truck dynamics model is employed as the prediction model in the optimization problem.

3.2.4 Feasibility and asymptotic convergence

According to the well-developed MPC schemes, the terminal control law $\kappa(x_e)$ and the terminal set $\mathcal{X}_f$ satisfy the following conditions:

A1: $\mathcal{X}_f \in \mathcal{X}_e$;
A2: $\kappa(0) = 0$, and $\kappa(x_e) \in \mathcal{U}_e$ for all $x_e \in \mathcal{X}_e$;
A3: $F(0) = 0$, and for all $x_e \in \mathcal{X}_f$, $F(x_e)$ satisfies

$$F(x_e(k+1)) - F(x_e(k)) \le -l(x_e(k), u_e(k)). \tag{33}$$

Lemma 1 (Th. 1 [41]) *Suppose that Problem 1 has a feasible solution at the time instant k. Then, 1): The Problem 1 remains feasible at the time intant k + 1; 2): The system state $x(k)$ asymptotically tracks the desired states x^d, i.e., $\lim_{k\to\infty}\|x_e(k)\| = 0$.*

Remark 7 Without considering differences in axle configuration or varying payload conditions, the proposed NMPC scheme is applicable to vehicles with identical vehicle dynamics (1) and tire models (2).

4 NTLT method

To reduce the computational burden of solving the optimization problem, the NTLT method is proposed.

4.1 Newton's type method

The inequality constraints (23e), (23f), and (23g) can be reformulated as [34]

$$f_b\left(x_{i|k}, u_{i-1|k}\right) \le 0,\ b = 1, \dots, \vartheta, \tag{34}$$

where ϑ is the number of inequality costraints.

In the framework of Newton's method, inequality constraints are typically transformed into a barrier cost function or a nonlinear algebraic equality constraint. Then, define the barrier function for (34) as

$$\phi\left(x_{i|k}, u_{i-1|k}\right) = \sum_{b=1}^{\vartheta} \xi_b \log\left(-f_b\left(x_{i|k}, u_{i-1|k}\right)\right), \tag{35}$$

where $\xi_b < 0$, $b \in \{1, 2, \dots, \vartheta\}$, are constants.

At the predicted time instants $i = 1, \dots, N-1$, the cost function can be expressed as

$$\mathcal{L}_{i|k}\left(u_{i-1|k}, x_{i|k}\right) = \left\|x_{i|k} - r_{i|k}\right\|_Q + \left\|\left(u_{e,i-1|k}\right)\right\|_R + \phi\left(x_{i|k}, u_{i-1|k}\right). \tag{36}$$

The cost function at the predicted time instant $i = N$ can be expressed as

$$\mathcal{L}_{N|k}\left(u_{N-1|k}, x_{N|k}\right) = \left\|x_{N|k} - x^d_{N|k}\right\|_P + \left\|\left(u_{e,N-1|k}\right)\right\|_R + \phi\left(x_{N|k}\right). \tag{37}$$

Thus, Problem 1 can be transformed into an optimization problem with only equality constraints as follows [34]:

Problem 3.

$$\underset{u^*(k)}{minimize} \left\|x_{0|k} - x^d_{0|k}\right\|_Q + \sum_{i=1}^{N} \mathcal{L}_{i|k}\left(u_{i-1|k}, x_{i|k}\right) \tag{38a}$$

subject to

$$x_{0|k} = x(k), \tag{38b}$$

$$x_{i|k} - f\left(x_{i-1|k}, u_{i-1|k}\right) = \mathbf{0}. \tag{38c}$$

Define the sequences $\left\{\lambda_{i|k} \in \mathbb{R}^{n_x}\right\}_{i=1}^{N}$ as the Lagrange multipliers for the difference equations (38c). Define the vector of unknown variables as $\mathcal{V}_{i|k} := \left[\lambda_{i|k}^T, u_{i-1|k}^T, x_{i|k}^T\right]^T \in \mathbb{R}^9$. The Hamiltonian function H of Problem 3 can be defined as

$$H\left(\mathcal{V}_{i|k}\right) = \sum_{i=1}^{N} \left\{\mathcal{L}_{i|k}\left(x_{i|k}, u_{i-1|k}\right) + \lambda_{i|k}\left[x_{i|k} - f\left(x_{i-1|k}, u_{i-1|k}\right)\right]\right\} \tag{39}$$

where $H_{u_{i-1|k}} = \partial H/\partial u_{i-1|k}$ and $H_{x_{i|k}} = \partial H/\partial x_{i|k}$.

The Karush-Kuhn-Tucker (KKT) conditions can be expressed as the following set of nonlinear algebraic equations

$$x_{i|k}^* - f\left(x_{i-1|k}^*, u_{i-1|k}^*\right) = \mathbf{0}, \tag{40a}$$

$$H_{u_{i-1|k}}^T\left(\lambda_{i|k}^*, u_{i-1|k}^*, x_{i|k}^*\right) = \mathbf{0}, \tag{40b}$$

$$H_{x_{i|k}}^T\left(\lambda_{i+1|k}^*, \lambda_{i|k}^*, u_{i-1|k}^*, x_{i|k}^*\right) = \mathbf{0}, \tag{40c}$$

where $i \in \{1, \cdots N\}$, $x_{0|k}^* = x(k)$, and $\lambda_{N+1|k}^* = \mathbf{0}$.

Note that $\left\{u_{i-1|k}^* \in \mathbb{R}^3\right\}_{i=1}^{N}$, $\left\{x_{i|k}^* \in \mathbb{R}^3\right\}_{i=1}^{N}$, and $\left\{\lambda_{i|k}^* \in \mathbb{R}^3\right\}_{i=1}^{N}$ represent the optimal sequences of the corresponding parameters.

The NT method is employed to solve the nonlinear algebraic equations (40). Then, (40) can be rewritten as

$$\varphi_{i|k}\left(x_{i-1|k}, \mathcal{V}_{i|k}, \lambda_{i+1|k}\right) = \mathbf{0},$$

where the subscript $i \in \{1, \ldots, N\}$, and $\mathcal{V}_{i|k} = \left[x_{i|k}^T, u_{i-1|k}^T, \lambda_{i|k}^T\right]^T$.

Furthermore, denote $\varphi := \left[\varphi_{1|k}^T, \varphi_{2|k}^T, \cdots, \varphi_{N|k}^T\right]^T$, and $\mathcal{V} := \left[\mathcal{V}_{1|k}^T, \mathcal{V}_{2|k}^T, \cdots, \mathcal{V}_{N|k}^T\right]^T$. Starting from an initial guess $\mathcal{V}^{(0)}$, the iteration of the full-step NT method is defined as

$$\mathcal{V}^{(\sigma+1)} = \mathcal{V}^{(\sigma)} - \Theta\left(\mathcal{V}^{(\sigma)}\right)^{-1} \varphi\left(\mathcal{V}^{(\sigma)}\right), \tag{41}$$

where the superscript (σ) denotes the iteration number, and $\Theta(\mathcal{V}) := \varphi'(\mathcal{V})$ represents the Jacobian matrix of φ with respect to $\mathcal{V}$, that is,

$$\Theta(\mathcal{V}) = \begin{bmatrix} \Theta_{1|k} & \mathcal{B}_1^R & \mathbf{0} & \mathbf{0} \\ \mathcal{B}_2^L & \Theta_{2|k} & \ddots & \mathbf{0} \\ \mathbf{0} & \ddots & \ddots & \mathcal{B}_{N-1}^R \\ \mathbf{0} & \mathbf{0} & \mathcal{B}_N^L & \Theta_{N|k} \end{bmatrix}, \tag{42}$$

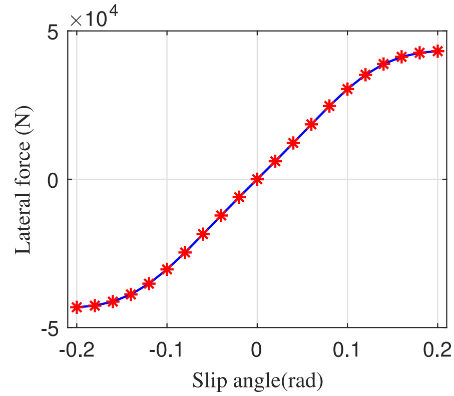

Fig. 5 Partitioning of the tire model

where $\Theta_{i|k} = \frac{\partial \varphi_i}{\partial \mathcal{V}_{i|k}}$,

$$\mathcal{B}_j^R = \frac{\partial \varphi_j}{\partial \mathcal{V}_{j+1|k}} = \begin{bmatrix} \mathbf{0} & \mathbf{0} \\ -\Psi\left(x_{j-1|k}\right) & \mathbf{0} \end{bmatrix}, \tag{43}$$

$$\mathcal{B}_j^L = \frac{\partial \varphi_j}{\partial \mathcal{V}_{j-1|k}} = \begin{bmatrix} \mathbf{0} & -\Psi\left(x_{j-1|k}\right) \\ \mathbf{0} & \mathbf{0} \end{bmatrix}, \tag{44}$$

and

$$\Psi\left(x_{i|k}\right) = \begin{bmatrix} 1 & t_s \gamma_{i|k} & t_s v_{y,i|k} \\ -t_s \gamma_{i|k} & 1 & -t_s v_{x,i|k} \\ 0 & 0 & 1 \end{bmatrix}. \tag{45}$$

Algorithm 1 The σth iteration of the NT method

Input: $\mathcal{V}^{(\sigma)}$, $x_{0|k}^{(\sigma)} = x_0$, $\lambda_{N+1|k}^{(\sigma)} = \mathbf{0}$
Output $\mathcal{V}^{(\sigma+1)}$
for $i = 1$ to N **do** in parallel
  $\varphi_{i|k}\left(x_{i-1|k}^{(\sigma)}, \mathcal{V}_{i|k}^{(\sigma)}, \lambda_{i+1}^{(\sigma)}\right) \leftarrow \mathcal{V}^{(\sigma)}$.
  $\Theta_{i|k}\left(\mathcal{V}_{i|k}^{(\sigma)}\right) \leftarrow \frac{\partial \varphi_{i|k}}{\partial \mathcal{V}_{i|k}}\Big|_{\left(\mathcal{V}_{i|k}^{(\sigma)}\right)}$.
end for
$\varphi\left(V^{(\sigma)}\right) \leftarrow \varphi_{i|k}\left(x_{i-1|k}^{(\sigma)}, V_{i|k}^{(\sigma)}, \lambda_{i+1|k}^{(\sigma)}\right)$.
$\Theta\left(V^{(\sigma)}\right) \leftarrow \Theta_{i|k}\left(V_{i|k}^{(\sigma)}\right)$.
$\mathcal{V}^{(\sigma+1)} = \mathcal{V}^{(\sigma)} - \Theta\left(\mathcal{V}^{(\sigma)}\right)\varphi\left(\mathcal{V}^{(\sigma)}\right)$.

The σ-th iteration of the NT method is outlined in Algorithm 1 [34]. The iteration process of the NT method for solving the nonlinear algebraic equations (40) is computationally expensive when evaluating $\varphi\left(\mathcal{V}^{(\sigma)}\right)$ and $\Theta\left(\mathcal{V}^{(\sigma)}\right)$. Particularly, for the nonlinear tire model (2), the tire force $f_t\left(\alpha_f\right)$, its first-order derivative $\partial f_t/\partial \alpha_f$, and its second-order derivative $\partial^2 f_t/\partial {\alpha_f}^2$ are computationally expensive due to the complex composite function.

Thus, to reduce the computational burden, an NTLT is proposed, where the values of the tire force $f_t\left(\alpha_f\right)$, its first-order derivative $\partial f_t/\partial\alpha_f$, and its second-order derivative $\partial^2 f_t/\partial\alpha_f{}^2$ are stored in a look-up table offline and searched online.

Algorithm 2 The σth iteration of the NTLT.

Input: $\mathcal{V}^{(\sigma)}$, $x_{0|k}^{(\sigma)}=x_0$, $\lambda_{N+1|k}^{(\sigma)}=\mathbf{0}$

Output $\mathcal{V}^{(\sigma+1)}$

Step 1: Search the index h of $\alpha\left(k\right)$ by the following hash function [35]:

$$h=\left\lfloor\left(\alpha_f\left(k\right)-\alpha_{fmin}\right)\times\frac{s}{\alpha_{fmax}-\alpha_{fmin}}\right\rfloor.$$

Step 2:

for $i=1$ to N **do** do in parallel

$$f_t\left(\hat{\alpha}_h\right),df_t/d\hat{\alpha}_h,d^2 f_t/d\hat{\alpha}_h^2\leftarrow u_{i|k}^{(\sigma)}$$

$$\bar{\varphi}_i\left(x_{i-1|k}^{(\sigma)},\mathcal{V}_{i|k}^{(\sigma)},\lambda_{i+1|k}^{(\sigma)}\right)\leftarrow\mathcal{V}^{(\sigma)},$$

$$\bar{\Theta}_i\left(\mathcal{V}_i^{(\sigma)}\right)\leftarrow\left.\frac{\partial\varphi_i}{\partial\mathcal{V}_i}\right|_{\left(\mathcal{V}_i^{(\sigma)}\right)},$$

where $f_t\left(\alpha_{f,i|k}\right)=f_t\left(\hat{\alpha}_h\right)$, $df_t/d\alpha_{f,i|k}=df_t/d\hat{\alpha}_h$, and $d^2f_t/d\alpha_{f,i|k}=d^2f_t/d\hat{\alpha}_h^2$.

end for

Step 3:

$$\bar{\varphi}\left(V^{(\sigma)}\right)\leftarrow\bar{\varphi}_{i|k}\left(x_{i-1|k}^{(\sigma)},V_{i|k}^{(\sigma)},\lambda_{i+1|k}^{(\sigma)}\right).$$

$$\bar{\Theta}\left(V^{(\sigma)}\right)\leftarrow\bar{\Theta}_i\left(V_{i|k}^{(\sigma)}\right).$$

$$\mathcal{V}^{(\sigma+1)}=\mathcal{V}^{(\sigma)}-\bar{\Theta}\left(\mathcal{V}^{(\sigma)}\right)\bar{\varphi}\left(\mathcal{V}^{(\sigma)}\right).$$

As shown in Fig. 5, divide the interval $\left[\alpha_{fmin},\alpha_{fmax}\right]$ into s equal segments, i.e.,

$$\alpha_h=\left[\alpha_{fmin}+h\delta,\alpha_{fmin}+\left(h+1\right)\delta\right],\tag{46}$$

where $h=0,\ldots,s-1$, and $\delta=\left(\alpha_{fmax}-\alpha_{fmin}\right)/s$ represents the grid step size.

In each segment α_h, an arbitrary point $\hat{\alpha}_h\in\alpha_h$ is selected offline. Then, the values of $f_t\left(\hat{\alpha}_h\right)$, $df_t/d\hat{\alpha}_h$, and $d^2f_t/d\hat{\alpha}_h^2$ are computed and stored in a hash table offline.

Then, the iteration process of the NTLT is presented in Algorithm 2, where the σ-th iteration is

$$\mathcal{V}^{(\sigma+1)}=\mathcal{V}^{(\sigma)}-\bar{\Theta}\left(\mathcal{V}^{(\sigma)}\right)^{-1}\bar{\varphi}\left(\mathcal{V}^{(\sigma)}\right).\tag{47}$$

Note that, in $\bar{\Theta}\left(\mathcal{V}^{(\sigma)}\right)$ and $\bar{\varphi}\left(\mathcal{V}^{(\sigma)}\right)$, the tire-related terms are determined according to Step 1.

Remark 8 Note that the proposed NTLT method is also applicable to inverse or quadratic barrier functions, as they have the same mechanism of handling constraints as the logarithmic function [18,34]. And a poor initial guess can hinder convergence. Therefore, a warm-start strategy is employed.

Table 2 Parameters of the truck

Parameters	Values	Parameters	Values
$m\ (kg)$	16695	I_z (kg m^2)	130421.8
$l_f\ (m)$	3.5	$l_r\ (m)$	1.5
B_f	4.579	C_f	1.5237
D_f	43226	E_f	−3.6477

Remark 9 Note that both feasibility and convergence of the proposed NMPC scheme are maintained due to the inherent robustness of the NMPC, while small uncertainties occur, such as model-plant mismatches caused by the vehicle load and the introduction of the look-up table, and external disturbances [42]. Therefore, the proposed NMPC is effective if the coefficients of the tire model vary within a small range.

5 Control strategy evaluation

To validate the proposed NMPC scheme and NTLT, co-simulations integrating MATLAB/Simulink and TruckSim are conducted. Simulations are performed on a desktop computer equipped with a 2.90 GHz Intel(R) Core(TM) i7–10700 processor.

5.1 Truck parameters

Truck parameters are presented in Table 2. The constraint sets of states and control inputs are, respectively,

$$\mathcal{X}:=\left\{x\in\mathbb{R}^3\left|\begin{array}{l}10m/s<v_x\leq 30m/s,\\-2m/s\leq v_y\leq 2m/s,\\-0.2rad/s\leq\gamma\leq 0.2rad's\end{array}\right.\right\},\tag{48}$$

and

$$\mathcal{U}=\left\{u\in\mathbb{R}^3\left|\begin{array}{l}-94000N\leq F_{xr}\leq 94000N,\\-0.174rad\leq\alpha_f\leq 0.174rad,\\-98000N\leq F_{yr}\leq 98000N\end{array}\right.\right\}.\tag{49}$$

The size of the look-up table is shown in Table 3. The larger the grid step size $\delta\ (rad)$, the less memory usage is required.

Table 3 The size of the Look-up table

δ (rad)	Size of the look-up table	Memory usage (Bytes)
0.001	399 × 3	9576
0.002	199 × 3	4776
0.004	99 × 3	2376

The constraint set of the desired state is

$$\mathcal{P} := \left\{ x^d \in \mathbb{R}^3 \left| \begin{array}{l} 10m/s \le v_x^d \le 30m/s, \\ -2m/s \le v_y^d \le 2m/s, \\ -0.2rad/s \le \gamma^d \le 0.2rad/s \end{array} \right. \right\}. \tag{50}$$

Δx^d is constrained as

$$\Delta\mathcal{P} := \left\{ \Delta x^d \in \mathbb{R}^3 \left| \begin{array}{l} -2.5m/s \le \Delta v_x^d \le 2.5m/s, \\ -0.2m/s \le \Delta v_y^d \le 0.2m/s, \\ -0.01rad/s \le \Delta\gamma^d \le 0.01rad/s \end{array} \right. \right\}. \tag{51}$$

The constraint set of the state (20) is

$$\mathcal{X}_e = \left\{ x_e \in \mathbb{R}^3 \left| \begin{array}{l} -20m/s \le v_{xe} \le 20m/s, \\ -4m/s \le v_{ye} \le 4m/s, \\ -0.4rad/s \le \gamma_e \le 0.4rad/s \end{array} \right. \right\}. \tag{52}$$

The constraints of the error input are

$$\begin{cases} u_{e1max} = \dfrac{F_{xmax}}{m} + \dfrac{\Delta v_{xmax}^d}{t_s} + \gamma_{max} v_{ymax}^d, \\ u_{e1min} = \dfrac{F_{xmin}}{m} + \dfrac{\Delta v_{xmin}^d}{t_s} + \gamma_{min} v_{ymax}^d, \\ u_{e2max} = \dfrac{F_{yfmax} + F_{yrmax}}{m} + \dfrac{\Delta v_{ymax}^d}{t_s} - \gamma_{min} v_{xmax}^d, \\ u_{e2min} = \dfrac{F_{yfmin} + F_{yrmin}}{m} + \dfrac{\Delta v_{ymin}^d}{t_s} - \gamma_{max} v_{xmax}^d, \\ u_{e3max} = \dfrac{l_f F_{yfmax} - l_r F_{yrmin}}{I_z} + \dfrac{\Delta\gamma_{max}^d}{t_s}, \\ u_{e3min} = \dfrac{l_f F_{yfmin} - l_r F_{yrmax}}{I_z} + \dfrac{\Delta\gamma_{min}^d}{t_s}. \end{cases} \tag{53}$$

Thus, in terms of (49) to (53), the constraint set (22) is

$$\mathcal{U}_e = \left\{ u_e \in \mathbb{R}^3 \left| \begin{array}{l} -56 \le u_{e1} \le 59, \\ -18.46 \le u_{e2} \le 14.5, \\ -2.49 \le u_{e3} \le 2.49 \end{array} \right. \right\}. \tag{54}$$

The validation of the truck model (3) during a J-turn maneuver is then implemented. The front wheel steering angle is shown in Fig. 6. The inputs of the truck model (3) are gathered from TruckSim under the J-turn maneuver. As shown in Fig. 7, the responses of the truck model (3) and the test truck are consistent during the J-turn maneuver, which demonstrates the effectiveness of the model [20].

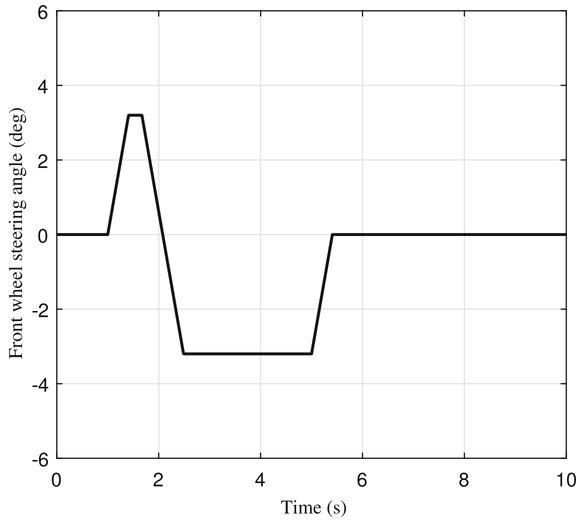

Fig. 6 Front wheel steering angle δ_f of the J-turn maneuver

Remark 10 Unmodeled dynamics of trucks (23c) arise due to the co-simulation implementation. As a result, the potential impact of system uncertainty is initially addressed.

5.2 Assessment of the weighting matrix of NMPC

The weighting matrix $Q = diag(q_1, q_2, q_3)$ directly affects the control performance. It can be assessed using performance indicators expressed in the form of root mean square error (RMSE)

$$\begin{cases} v_{xp} = \sqrt{\sum\limits_{k=1}^{n} \left[v_x^d(k) - v_x(k) \right]^2}, \\ v_{yp} = \sqrt{\sum\limits_{k=1}^{n} \left[v_y^d(k) - v_y(k) \right]^2}, \\ \gamma_p = \sqrt{\sum\limits_{k=1}^{n} \left[\gamma^d(k) - \gamma(k) \right]^2}, \end{cases} \tag{55}$$

where n is the length of the data. By (55), a smaller RMSE indicates better tracking performance. The assessment of the weighting matrix is conducted under a lane-changing scenario [43]. The prediction horizon

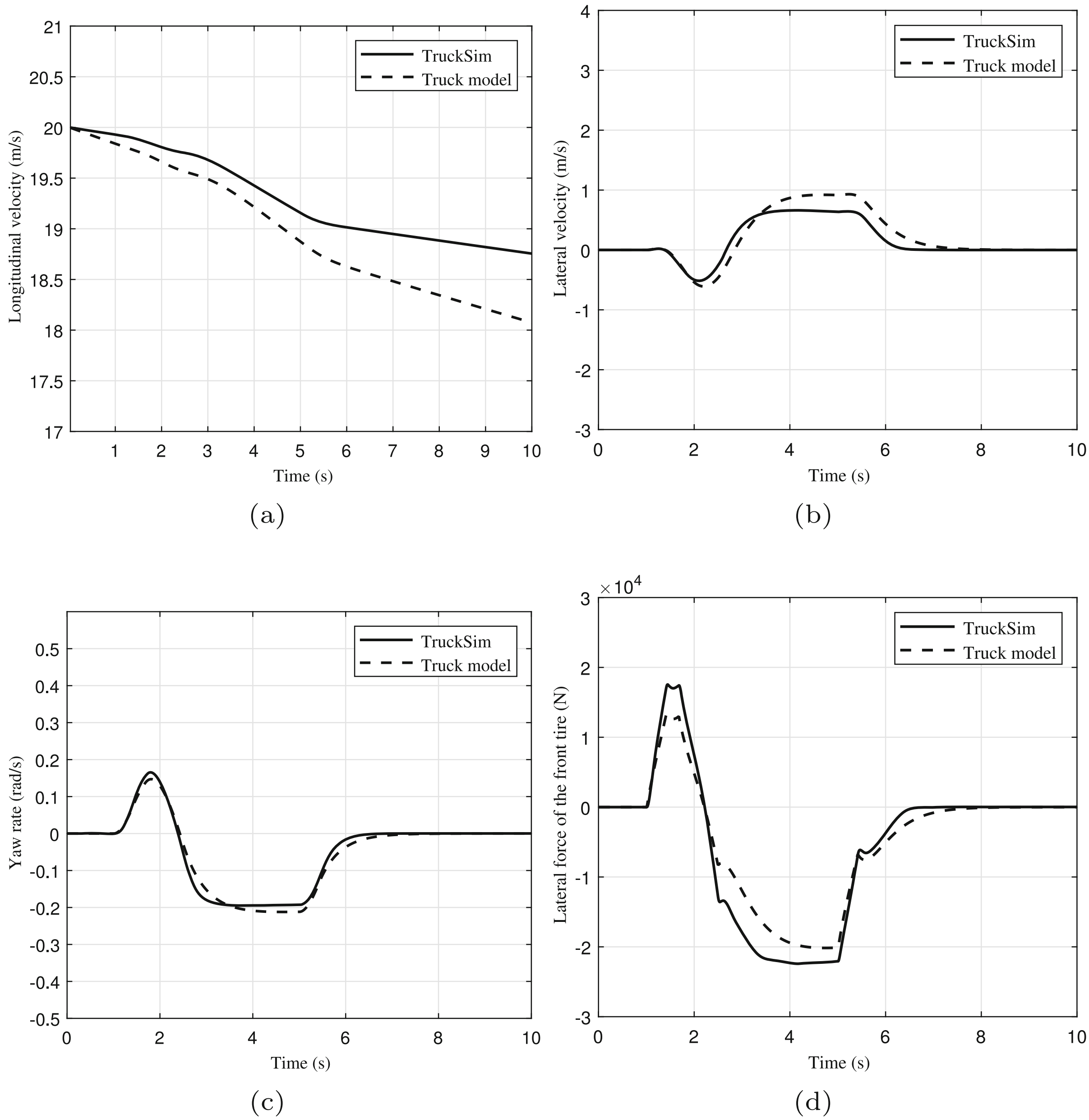

Fig. 7 J-turn maneuver: **a** longitudinal velocity, **b** lateral velocity, **c** yaw rate, **d** lateral force of the front tire

is $N = 10$ with a sampling time of $t_s = 0.05$s. The assessment results for the weighting matrix are shown in Fig. 8. A smaller area enclosed by the three indicators indicates better control performance.

Thus, to achieve optimal control performance, the weighting matrices are chosen as

$$Q = diag(1.5 \times 10^3, 5 \times 10^3, 1.5 \times 10^6), \tag{56}$$

and

$$R = diag(1 \times 10^{-10}, 1 \times 10^{-2}, 1 \times 10^{-6}). \tag{57}$$

According to (52) and (54), the pairs (c_j, d_j) are

$$\begin{cases} c_1 = diag\,(1/20, 1/4, 1/0.4)\,, d_1 = 0, \\ c_2 = -diag\,(1/20, 1/4, 1/0.4)\,, d_2 = 0, \\ c_3 = 0, d_3 = diag\,(1/59, 1/14.5, 1/2.49)\,, \\ c_4 = 0, d_4 = -diag\,(1/56, 1/18.46, 1/2.49)\,. \end{cases} \tag{58}$$

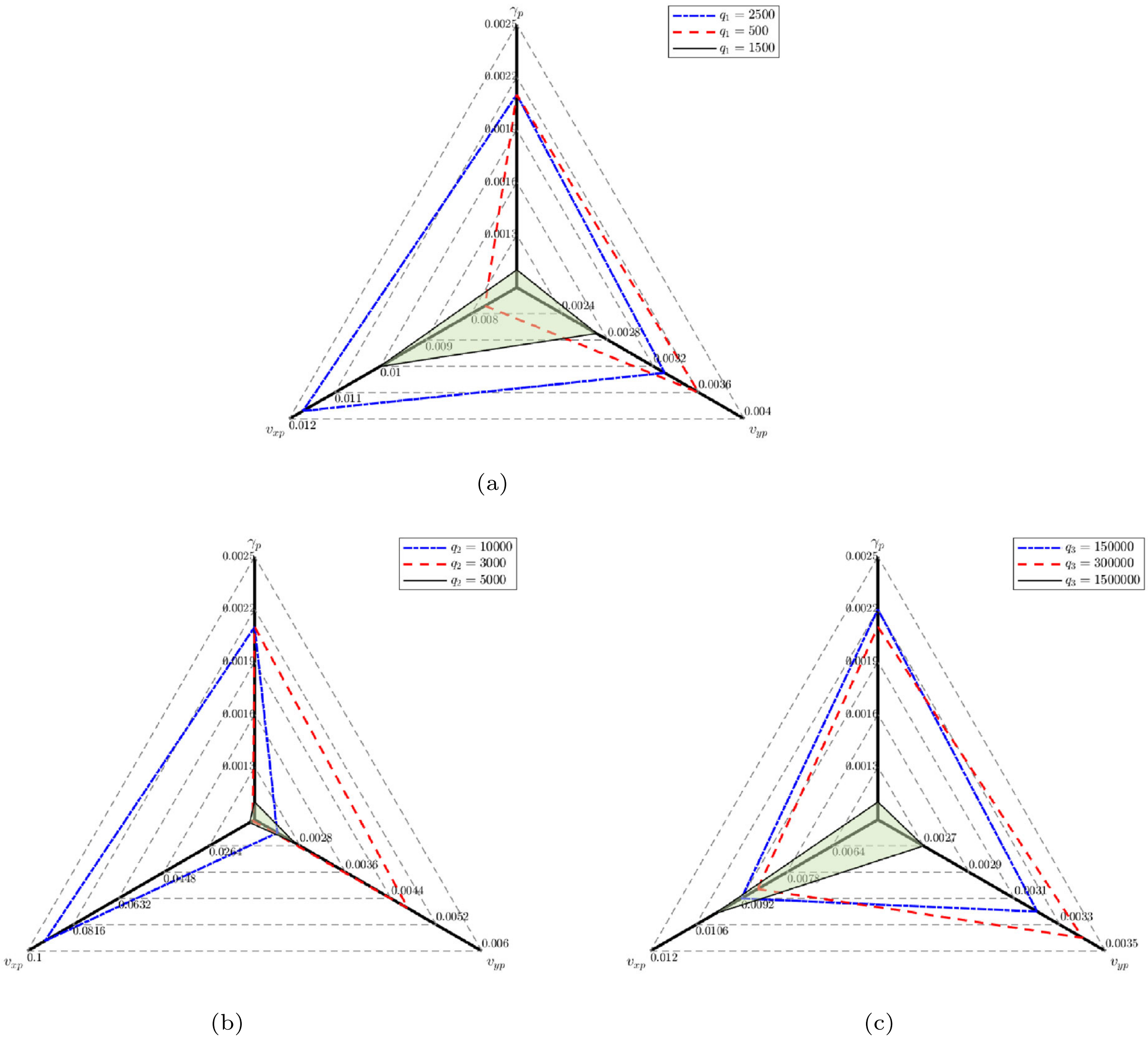

Fig. 8 Results of the weighting matrix assessment: **a** assessment on q_1 (with $q_2 = 5 \times 10^3$ and $q_3 = 1.5 \times 10^6$), **b** assessment on q_2 (with $q_1 = 1.5 \times 10^3$ and $q_3 = 1.5 \times 10^6$), **c** assessment on q_3 (with $q_1 = 1.5 \times 10^3$ and $q_2 = 1.5 \times 10^6$)

Then, by solving Problem 2, the terminal penalty function is

$$F\left(x_p\right) = x_p^T P x_p, \tag{59}$$

where

$$P = \begin{bmatrix} 2.8292 \times 10^7 & * & * \\ 3.0803 \times 10^5 & 2.6477 \times 10^8 & * \\ -5.1186 \times 10^5 & 3.3141 \times 10^8 & 7.5004 \times 10^8 \end{bmatrix}. \tag{60}$$

5.3 Verification of the proposed NMPC

In this section, two cases are conducted to evaluate the effectiveness of the proposed NMPC. The grid step is set to $\delta = 0.001$rad in both Case 1 and Case 2. The condition for terminating the iteration of the NTLT algorithm is

$$\left\| \mathcal{V}^{(\sigma+1)} - \mathcal{V}^{(\sigma)} \right\| \leq \Delta \tag{61}$$

where $\Delta = 10^{-6}$.

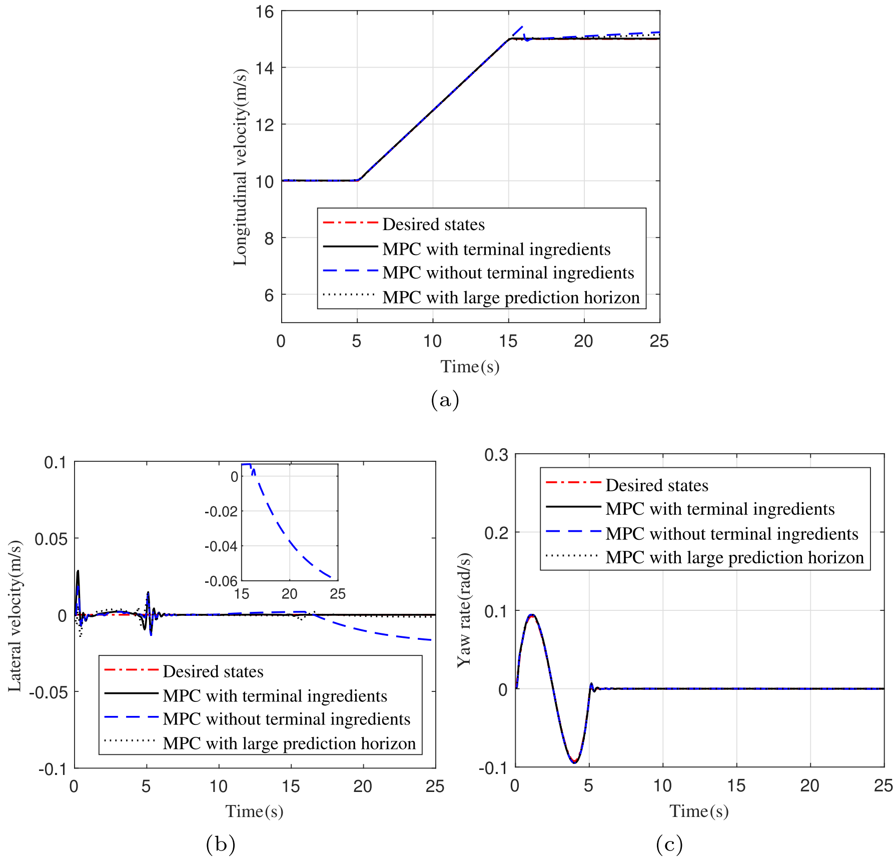

Fig. 9 State responses of Case 1: **a** longitudinal velocity, **b** lateral velocity, **c** yaw rate

5.3.1 Case 1: Accelerated lane changing scenario

For comparison, an NMPC without guaranteed convergence is also designed [18–23], where the terminal constraint and terminal penalty function are omitted. Furthermore, an NMPC with a large prediction horizon is also introduced [31]. The desired longitudinal velocity profile is predefined. The initial state $x(0) = \begin{bmatrix} 10\ 0\ 0 \end{bmatrix}^T$. The desired lateral velocity is 0m/s. The reference trajectory is defined as [44]

$$Y^d(t) = 4\left[10\left(\frac{v_x^d(t)}{50}\right)^3 - 15\left(\frac{v_x^d(t)}{50}\right)^4 + 6\left(\frac{v_x^d(t)}{50}\right)^5\right]. \tag{62}$$

The simulation results of Case 1 are shown in Figs. 9 and 10. The dashed line represents the desired states. The solid line represents the responses of the NMPC with terminal ingredients. The dashed line represents the responses of the NMPC without terminal ingredients. The dotted line represents the responses of the NMPC with a large prediction horizon ($N = 30$). In Fig. 9a, the proposed NMPC successfully tracks the desired longitudinal velocity. In contrast, for the NMPC without terminal ingredients, the longitudinal velocity responses diverge from the desired value after 15 s. In Fig. 9b, the lateral velocity of the proposed controller converges to 0m/s. In contrast, the NMPC without terminal ingredients cannot track the desired value. The NMPC with a large prediction horizon can guarantee that the vehicles track the desired states, while a larger computational time is established compared with the proposed NMPC. In Fig. 9c, all controllers successfully track the desired yaw rate. Moreover, all of controllers exhibit a low RMSE, as shown in Table 4. However, as shown in Fig. 10a, for the NMPC without terminal ingredients, the longitudinal force of the rear tire exhibits a peak. Consequently, the truck experiences weak handling stability due to large accelerations and decelerations.

Remark 11 Note that the NMPC without terminal ingredients may fail to ensure convergence of the vehicle tracking trajectory error in certain cases, such as

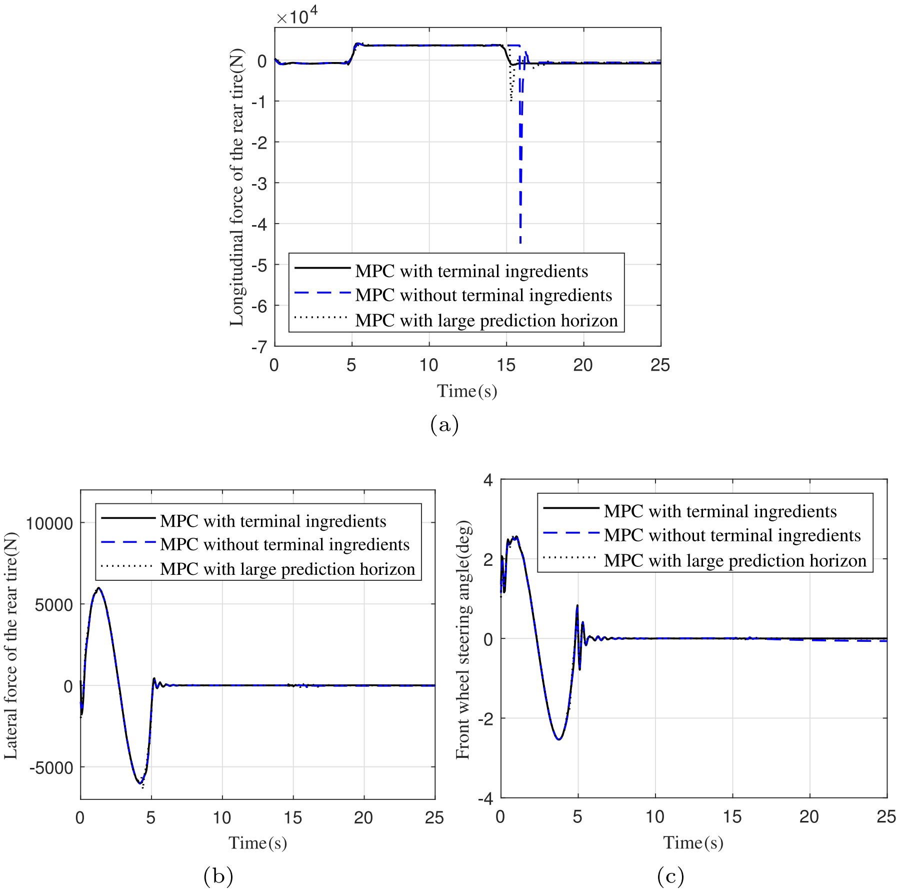

Fig. 10 Input responses of Case 1: **a** longitudinal force of the rear tire, **b** lateral force of the rear tire, **c** front wheel steering angle

Table 4 RMSE of the control performance of Case 1

NMPC	v_{xp}	v_{yp}	γ_p
With terminal ingredients	0.0106	0.0027	0.0011
Without terminal ingredients	0.0624	0.0068	0.0011
With large prediction horizon	0.0499	0.0023	0.0010

case 1 presented in this paper. However, it is capable of achieving the desired vehicle tracking performance in most situations.

5.3.2 *Case 2: Decelerated lane changing scenario*

In this case, the proposed NMPC is evaluated in comparison to an NMPC without constraints, highlighting the importance of considering constraints. The desired longitudinal velocity profile is predefined as shown in Fig. 11a. The desired lateral velocity is set to 0m/s. The reference trajectory can be defined by (62). The initial state $x(0) = \left[20\ 0\ 0\right]^T$.

The simulation results for Case 2 are presented in Figs. 11 and 12, where the solid red lines denote the values of the input constraints. The dashed red line represents the reference trajectory. The solid black line represents the responses of the NMPC with constraints. The dashed line represents the responses of the NMPC without constraints.

As shown in Table 5 and Fig. 11, compared with the NMPC without constraints, the proposed scheme exhibits a smaller RMSE and steady-state errors. Note that the control inputs of the NMPC without constraints do not satisfy the constraints in Fig. 12c. The simulation results indicate that the proposed controller is effective for trajectory tracking of ATs.

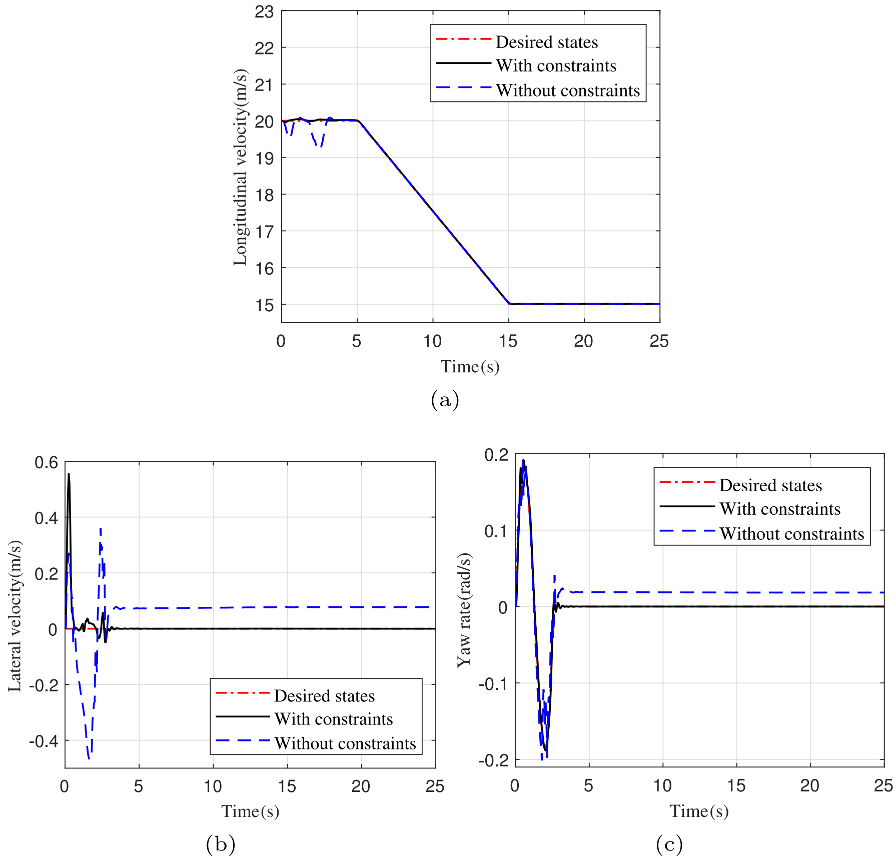

Fig. 11 State responses of Case 2: **a** longitudinal velocity, **b** lateral velocity, **c** yaw rate

5.4 Verification of the NTLT

5.4.1 Case 3: Results of different prediction horizons

To verify the performance of the proposed method compared to the NT method, the number of iterations is set to 20, and $\delta = 0.001$ rad. Simulations with different prediction horizons ($h = 15$, $h = 20$, $h = 30$, $h = 50$) are performed, grouped into four sets, labeled as 1, 2, 3, and 4.

In Fig. 13, the RMSE of the control performance of both methods are similar. In Fig. 14a, the computational time increases with the prediction horizon. The speed-up of the proposed NTLT compared to the NT method can be calculated as follows

$$\varepsilon(k) = \frac{t_{NT}(k) - t_{NTLT}(k)}{t_{NT}(k)} \times 100\%. \tag{63}$$

where ε is the speed-up, t_{NT} is the computational time of the NT method, and t_{NTLT} is the computational time of the proposed NTLT. As shown in Fig. 14b, the proposed NTLT achieves a speed-up from 20% to 35%.

5.4.2 Case 4: Results of different number of iterations

To verify the performance of the proposed method compared to the NT method, the prediction horizon is set to 10, and $\delta^1 = 0.001$ rad. Simulations with different number of iterations {15, 20, 30, 50, 100} are performed. Note that this case is conducted solely to demonstrate the effectiveness of reducing computational time by introducing the look-up table instead of tire functions. In vehicle engineering applications, the conditions for terminating the iteration should be adaptable.

As shown in Fig. 15, the RMSE of both methods are similar, indicating that the proposed method is effective for trajectory tracking. Furthermore, the RMSE decreases with an increasing number of iterations, indicating that the proposed method converges towards the optimal solution. In Fig. 16a, the computational time increases with the number of iterations. In Fig. 16b, the proposed NTLT can achieve a speed-up of 20% to 35%.

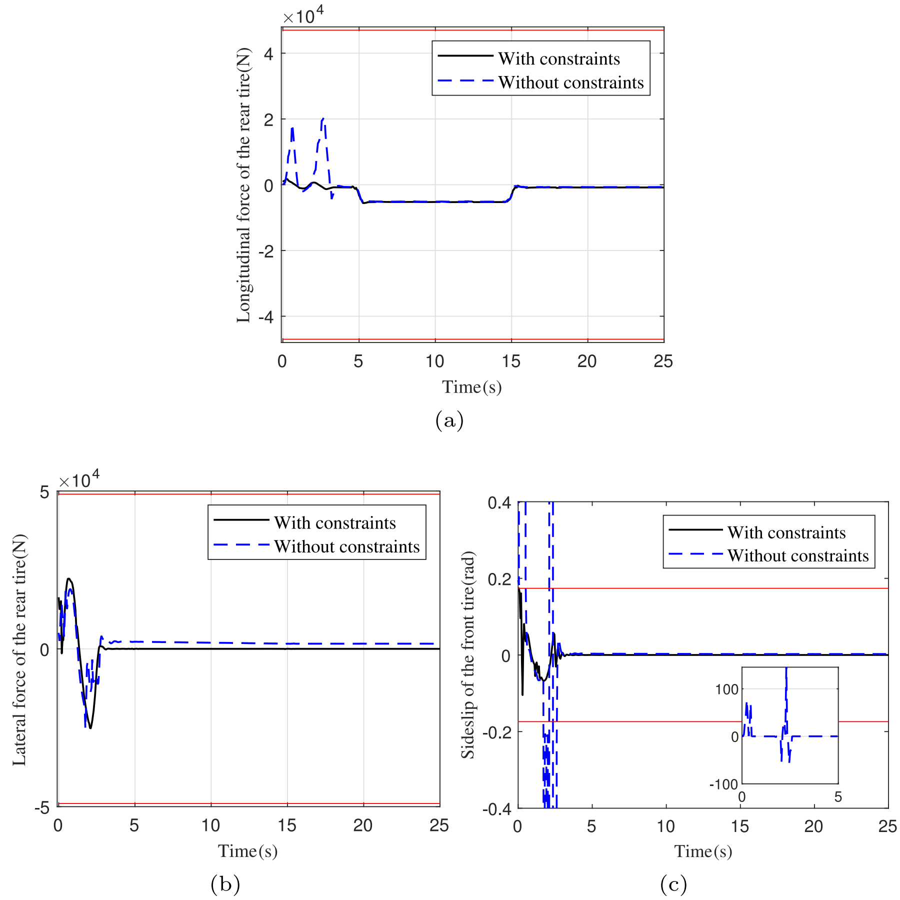

Fig. 12 Input responses of Case 2: **a** longitudinal force of the rear tire, **b** lateral force of the rear tire, **c** sideslip angle of the front tire

Table 5 RMSE of the control performance of Case 2

NMPC	v_{xp}	v_{yp}	γ_p
With constraints	0.0148	0.0490	0.0025
Without constraints	0.1289	0.1120	0.0200

6 Conclusion

This paper proposed an NMPC scheme for the reference trajectory tracking of ATs. Initially, the truck dynamics considering the coupled longitudinal, lateral, and yaw motions and the Magic Formula tire model were established. The problem of tracking the reference trajectory was transformed into a regulation problem. The optimization problem was then formulated with terminal ingredients derived based on the PLDI approach. Both the feasibility and the asymptotic convergence of the proposed NMPC scheme were proven.

Furthermore, the NTLT was proposed for solving the optimization problem, in which relevant tire values were computed offline and searched online. Simulation results showed that the proposed NMPC scheme can effectively and asymptotically track the desired states. The NTLT notably enhanced computational efficiency, i.e., achieving a speed-up of 20% to 35% compared to the NT method.

The validation of the NTLT is conducted through simulations. It is important to note that lookup tables introduce discontinuities, which affect the search direction and, consequently, the convergence of the NT method. In this study, we focused solely on the feasibility of the NTLT for truck engineering. Future research should rigorously prove the convergence of the NTLT.

Fig. 13 Simulation results of Case 3: **a** Longitudinal velocity, **b** Lateral velocity, **c** Yaw rate

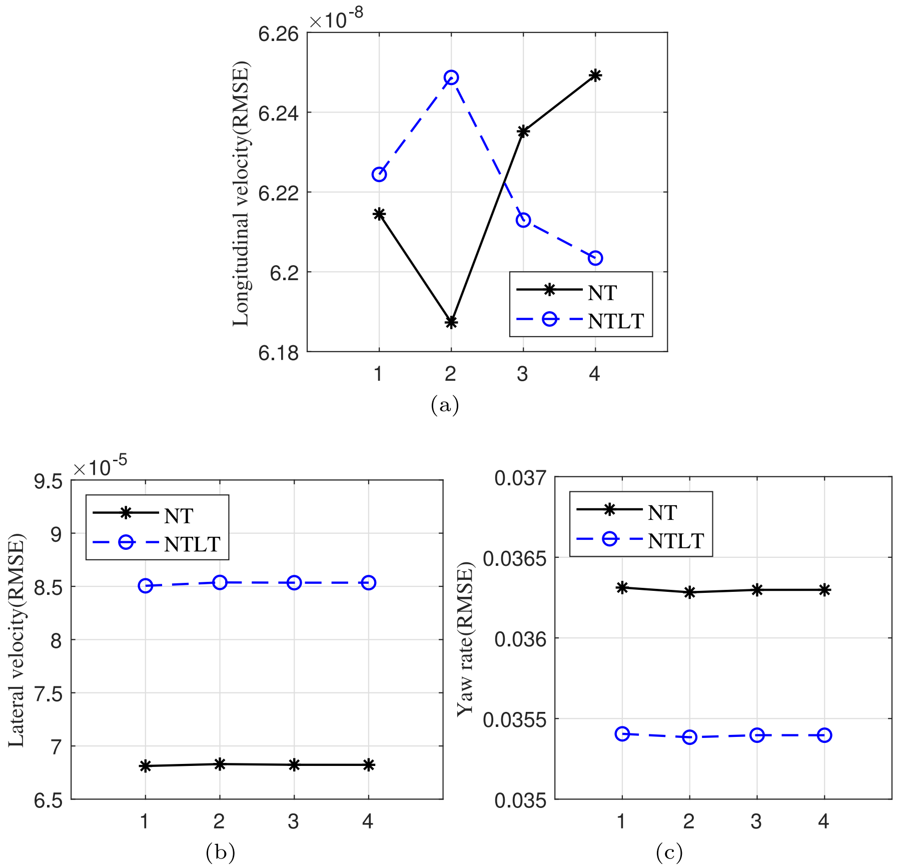

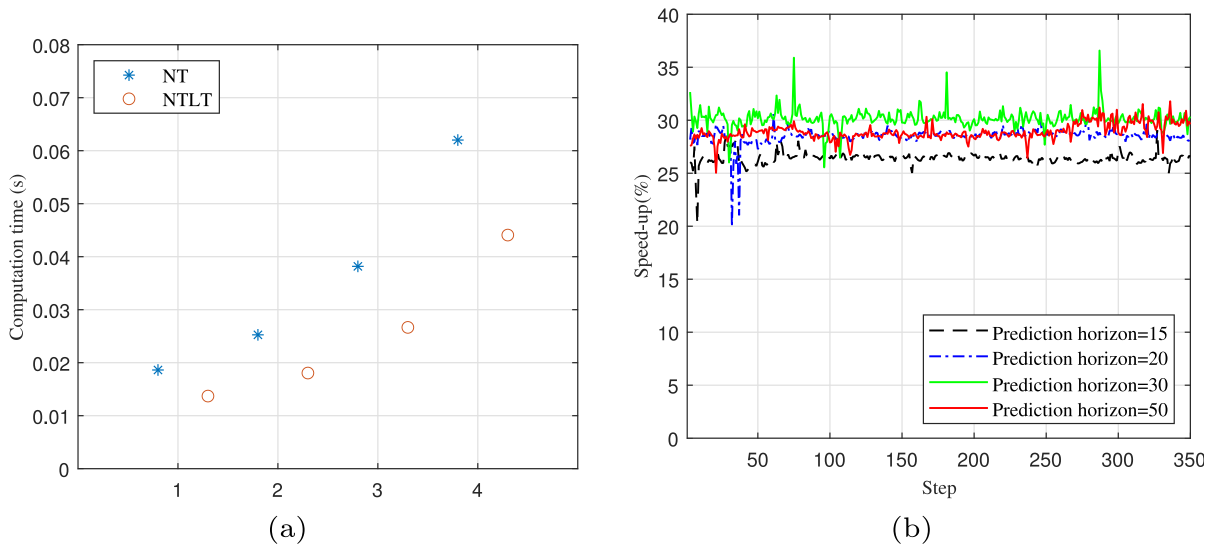

Fig. 14 Computation time of Case 3: **a** Average computation time, **b** Speed-up

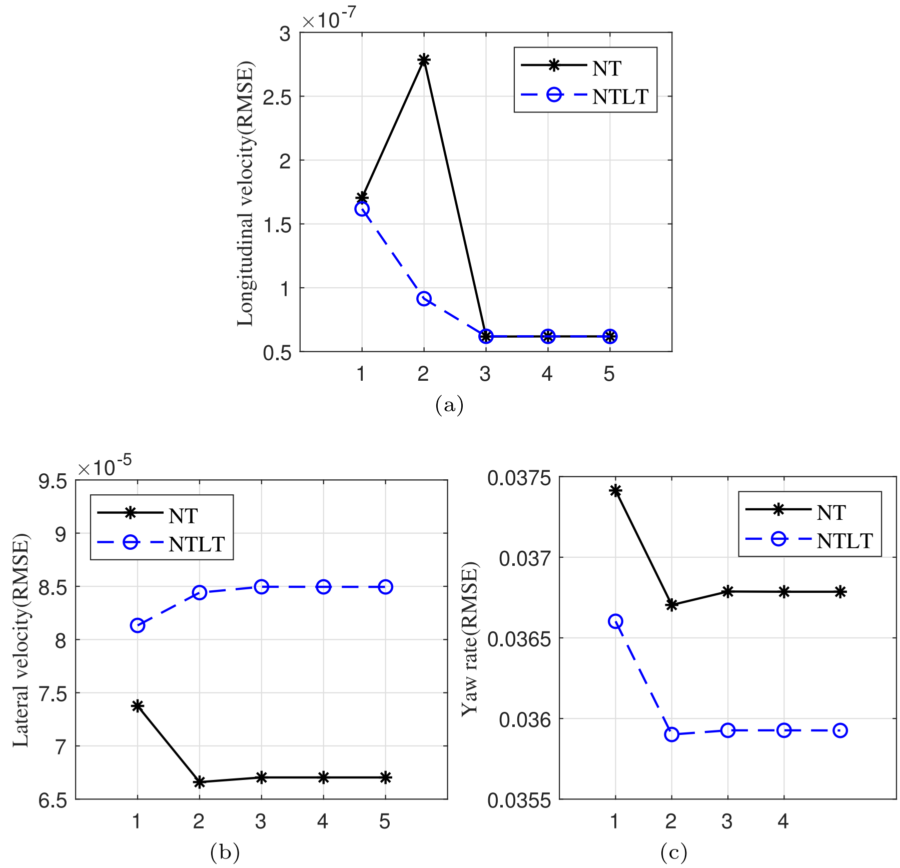

Fig. 15 Simulation results of Case 4: **a** Longitudinal velocity, **b** Lateral velocity, **c** Yaw rate

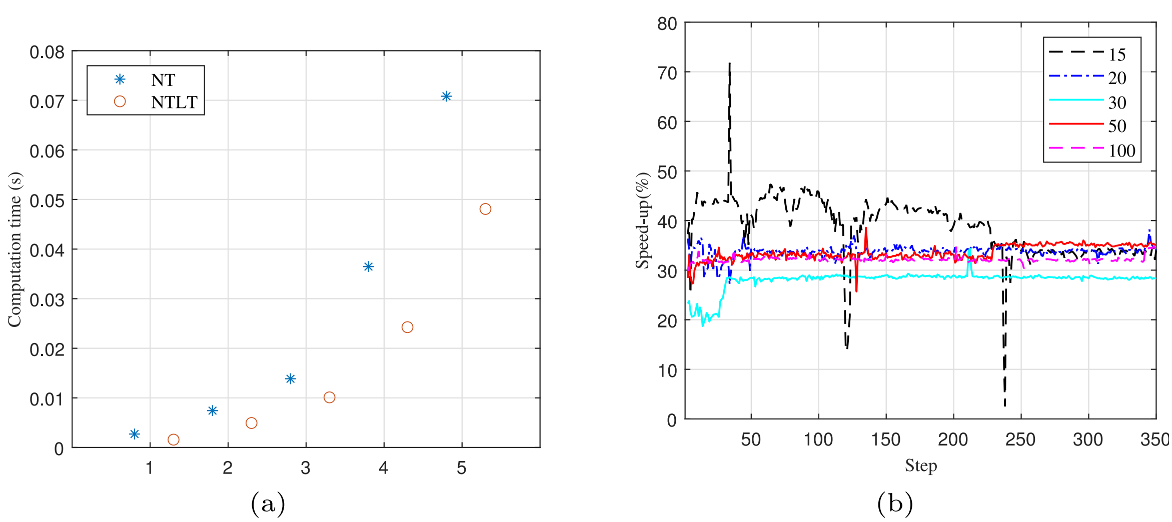

Fig. 16 Computation time of Case 4: **a** Average computation time, **b** Speed-up

Acknowledgements This work was supported by the National Natural Science Foundation of China (No. 62473167) and the Natural Science Foundation of Jilin Province (No. 2024040207-9GH).

Funding The authors have not disclosed any funding.

Data Availability Statement No datasets were generated or analysed during the current study.

Declarations

Conflict of interest The authors declare that they have no Conflict of interest.

References

1. Kuutti, S., Bowden, R., Jin, Y., Barber, P., Fallah, S.: A survey of deep learning applications to autonomous vehicle control. IEEE Trans. Intell. Transp. Syst. **22**(2), 712–733 (2021)
2. Wang, Y., Wei, C., Li, S., Sun, J., Cao, J.: A convex trajectory planning method for autonomous vehicles considering kinematic feasibility and bi-state obstacles avoidance effectiveness. IEEE Trans. Veh. Technol. **73**(7), 9575–9590 (2024)
3. Jiang, L., Deng, Y., Jiang, Z., He, R., Yu, H., Xu, W., Meng, J.: Accurate data-driven sliding mode parking control for autonomous ground vehicles with efficient trajectory planning in dynamic industrial scenarios. Nonlinear Dyn. **112**(13), 11195–11216 (2024)
4. Li, W., Ding, H., Xu, N., Song, Z., Zhang, J.: A time and energy efficient merging control for platoon formation of connected and automated electric vehicles at on-ramps. Nonlinear Dyn. **112**(5), 3619–3642 (2024)
5. Shi, S., Li, L., Mu, Y., Chen, G.: Stable headway prediction of vehicle platoon based on the 5-degree-of-freedom vehicle model. Proc. Inst. Mech. Eng. Part D J. Automob. Eng. **233**(6), 1570–1585 (2019)
6. Gong, Y., Zhu, W.-X.: Robust control scheme for the mixed platoon system with time-varying information topologies and inaccurate state information. Nonlinear Dyn. **112**, 22057–22085 (2024)
7. Li, W., Yu, S., Tan, L., Li, Y., Chen, H., Yu, J.: Integrated control of path tracking and handling stability for autonomous ground vehicles with four-wheel steering. Proc. Inst. Mech. Eng. Part D J. Automob. Eng. **239**(1), 315–326 (2025)
8. Taghavifar, H., Rakheja, S.: Path-tracking of autonomous vehicles using a novel adaptive robust exponential-like-sliding-mode fuzzy type-2 neural network controller. Mech. Syst. Signal Process. **130**, 41–55 (2019)
9. Akermi, K., Chouraqui, S., Boudaa, B.: Novel smc control design for path following of autonomous vehicles with uncertainties and mismatched disturbances. Int. J. Dyn. Control **8**(1), 254–268 (2020)
10. Lu, L., Jiao, X., Zhang, T.: Adaptive terminal sliding mode trajectory tracking control with fixed-time prescribed performance considering rollover stability of autonomous vehicles. Int. J. Robust Nonlinear Control **34**(7), 4554–4575 (2024)
11. Hosseinnajad, A., Mohajer, N., Nahavandi, S.: Barrier Lyapunov function-based backstepping controller design for path tracking of autonomous vehicles. J. Intell. Robot. Syst. **110**(3), 1–15 (2024)
12. Wang, Z., Liang, Z., Ding, Z.: Observer-based prescribed performance path-following control for autonomous ground vehicles via error shifting method. Nonlinear Dyn. **112**(12), 10061–10080 (2024)
13. Chen, G., Zhao, X., Gao, Z., Hua, M.: Dynamic drifting control for general path tracking of autonomous vehicles. IEEE Trans. Intell. Veh. **8**(3), 2527–2537 (2023)
14. Yu, S., Hirche, M., Huang, Y., Chen, H., Allgöwer, F.: Model predictive control for autonomous ground vehicles: a review. Autonom. Intell. Syst. **1**, 1–17 (2021)
15. Cai, M., Wu, W., Zhou, X.: Trajectory tracking control for autonomous parking based on adaptive reduced-horizon model predictive control. In: 2022 IEEE International Conference on Networking, Sensing and Control (ICNSC), pp. 1–6 (2022)
16. Mi, Y., Shao, K., Liu, Y., Wang, X., Xu, F.: Integration of motion planning and control for high-performance automated vehicles using tube-based nonlinear mpc. IEEE Trans. Intell. Veh. **9**(2), 3859–3875 (2024)
17. Chu, D., Li, H., Zhao, C., Zhou, T.: Trajectory tracking of autonomous vehicle based on model predictive control with pid feedback. IEEE Trans. Intell. Transp. Syst. **24**(2), 2239–2250 (2023)
18. Xu, F., Zhang, X., Chen, H., Hu, Y., Wang, P., Qu, T.: Parallel nonlinear model predictive controller for real-time path tracking of autonomous vehicle. IEEE Trans. Ind. Electron. **71**(12), 16503–16513 (2024)
19. Rokonuzzaman, M., Mohajer, N., Nahavandi, S., Mohamed, S.: Model predictive control with learned vehicle dynamics for autonomous vehicle path tracking. IEEE Access **9**, 128233–128249 (2021)
20. Li, Z., Chen, H., Liu, H., Wang, P., Gong, X.: Integrated longitudinal and lateral vehicle stability control for extreme conditions with safety dynamic requirements analysis. IEEE Trans. Intell. Transp. Syst. **23**(10), 19285–19298 (2022)
21. Nguyen, H.D., Kim, D., Son, Y.S., Han, K.: Linear time-varying mpc-based autonomous emergency steering control for collision avoidance. IEEE Trans. Veh. Technol. **72**(10), 12713–12727 (2023)
22. Wu, H., Si, Z., Li, Z.: Trajectory tracking control for four-wheel independent drive intelligent vehicle based on model predictive control. IEEE Access **8**, 73071–73081 (2020)
23. Zhang, Y., Liang, X., Ge, S.S., Gao, B., Chen, H.: Manoeuver planning, synchronized optimization and boundary motion control for autonomous vehicles under cut-in scenarios. Nonlinear Dyn. **111**(8), 6923–6939 (2023)
24. Lee, J., Hwang, Y., Choi, S.B.: Robust tube-mpc based steering and braking control for path tracking at high-speed driving. IEEE Trans. Veh. Technol. **72**(12), 15301–15316 (2023)
25. Hu, K., Cheng, K.: Robust tube-based model predictive control for autonomous vehicle path tracking. IEEE Access **10**, 134389–134403 (2022)
26. Wu, X., Wei, C., Zhang, H., Jiang, C., Hu, C.: Path-tracking and lateral stabilization for automated vehicles via learning-

based robust model predictive control. IEEE Trans. Veh. Technol. 1–12 (2024)
27. Feng, Y., Yu, S., Sheng, E., Li, Y., Shi, S., Yu, J., Chen, H.: Distributed mpc of vehicle platoons considering longitudinal and lateral coupling. IEEE Trans. Intell. Transp. Syst. **25**(3), 2293–2310 (2024)
28. Shen, C., Shi, Y.: Distributed implementation of nonlinear model predictive control for auv trajectory tracking. Automatica **115**, 108863 (2020)
29. Shen, C., Shi, Y., Buckham, B.: Trajectory tracking control of an autonomous underwater vehicle using Lyapunov-based model predictive control. IEEE Trans. Ind. Electron. **65**(7), 5796–5805 (2018)
30. Wang, D., Pan, Q., Shi, Y., Hu, J., Records, C.Z.: Efficient nonlinear model predictive control for quadrotor trajectory tracking: algorithms and experiment. IEEE Trans. Cybern. **51**(10), 5057–5068 (2021)
31. Berntorp, K., Quirynen, T.U.R., Cairano, S.D.: Trajectory tracking for autonomous vehicles on varying road surfaces by friction-adaptive nonlinear model predictive control. Veh. Syst. Dyn. **58**(5), 705–725 (2020)
32. Grüne, L.: Nmpc without terminal constraints. IFAC Proc. Vol. **45**, 1–13 (2012)
33. Chen, Y., Scarabottolo, N., Bruschetta, M., Beghi, A.: Efficient move blocking strategy for multiple shooting-based non-linear model predictive control. IET Control Theory Appl. **14**(2), 343–351 (2020)
34. Deng, H., Ohtsuka, T.: A parallel newton-type method for nonlinear model predictive control. Automatica **109**, 108560 (2019)
35. Zhang, J., Chin, K.-S., Ławryńczuk, M.: Nonlinear model predictive control based on piecewise linear Hammerstein models. Nonlinear Dyn. **92**(3), 1001–1021 (2018)
36. Zheng, H., Zou, T., Hu, J., Yu, H.: An offline optimization and online table look-up strategy of two-layer model predictive control. IEEE Access **6**, 47433–47441 (2018)
37. Yu, S., Li, W., Li, Y., Chen, H., Chu, H., Lin, B., Yu, J.: Nonlinear predictive control of active four-wheel steering vehicles. Int. J. Control Autom. Syst. **21**(10), 3336–3347 (2023)
38. Frasch, J.V., Sager, S., Diehl, M.: A parallel quadratic programming method for dynamic optimization problems. Math. Program. Comput. **7**, 289–329 (2015)
39. Zhang, B., Shi, S., Yu, S., Yu, J., Li, Y., Meng, F., Lin, N.: Establishment of a two-axis commercial vehicle 6-dof prediction model for nonlinear mpc controller. Proc. Inst. Mech. Eng. Part D J. Automob. Eng. **238**(10–11), 2891–2904 (2024)
40. Belrzaeg, M., Ahmed, A.A., Almabrouk, A.Q., Khaleel, M.M., Ahmed, A.A., Almukhtar, M.: Vehicle dynamics and tire models: an overview. World J. Adv. Res. Rev. **12**(1), 331–348 (2021)
41. Yu, S., Li, X., Chen, H., Allgöwer, F.: Nonlinear model predictive control for path following problems. Int. J. Robust Nonlinear Control **25**(8), 1168–1182 (2014)
42. Yu, S., Reble, M., Chen, H., Allgöwer, F.: Inherent robustness properties of quasi-infinite horizon nonlinear model predictive control. Automatica **50**(9), 2269–2280 (2014)
43. Yue, M., Hou, X., Zhao, X., Wu, X.: Robust tube-based model predictive control for lane change maneuver of tractor-trailer vehicles based on a polynomial trajectory. IEEE Trans. Syst. Man Cybern. Syst. **50**(12), 5180–5188 (2018)
44. Wang, J., Wang, J., Wang, R., Hu, C.: A framework of vehicle trajectory replanning in lane exchanging with considerations of driver characteristics. IEEE Trans. Veh. Technol. **66**(5), 3583–3596 (2016)